International Journal of Solids and Structures 188–189 (2020) 133–140

Contents lists available at ScienceDirect

International Journal of Solids and Structures

journal homepage: www.elsevier.com/locate/ijsolstr

Buckling of a stiff thin film on a bi-layer compliant substrate of finite thickness

Chengjun Wang[a,1], Shun Zhang[a,1], Shuang Nie[a], Yipin Su[b], Weiqiu Chen[a,*], Jizhou Song[a,*]

[a] Department of Engineering Mechanics, Soft Matter Research Center, and Key Laboratory of Soft Machines and Smart Devices of Zhejiang Province, Zhejiang University, Hangzhou 310027, China
[b] School of Mathematics, Statistics and Applied Mathematics, NUI Galway, University Road, Galway, Ireland

ARTICLE INFO

Article history:
Received 16 May 2019
Revised 26 September 2019
Accepted 14 October 2019
Available online 15 October 2019

Keywords:
Buckling
Thin film
Bi-layer substrate
Finite thickness

ABSTRACT

The buckling of a stiff thin film on a compliant substrate has been widely studied over the past decade due to its wide applications such as stretchable electronics, micro- and nano-metrology, and surface engineering. Instead of a single-layer compliant substrate, a bi-layer compliant substrate is usually encountered in practical applications. In this paper, the buckling of a stiff thin film on a bi-layer compliant substrate of finite thickness is studied theoretically, numerically and experimentally. The theoretical models based on the small-deformation theory and the simple finite-deformation theory accounting for the geometry change by using the energy method are both developed and presented. The good agreement among theoretical predictions, finite element analysis and experimental measurements of the buckling behavior validates the theoretical model. The influences of finite thickness of the bi-layer substrate and substrate modulus ratio on the buckling wavelength and critical buckling strain are systematically investigated. The buckling configurations at various applied strains are also measured to further validate the theoretical model. These results shed light on the influence of finite substrate thickness on buckling of the bi-layer substrate-supported thin films and are helpful to provide design guidelines in practical applications.

1. Introduction

The pioneering work of Bowden et al. (1998) showed that a stiff thin film adhered onto a compliant substrate can buckle into a well-defined, controllable surface pattern under in-plane compression. This phenomenon has attracted much attention due to its wide applications ranging from stretchable electronics (Khang et al., 2006; Kim et al., 2008; Song, 2015; Song et al., 2015; Zhang et al., 2015), micro- and nano-metrology (Stafford et al., 2004; Wilder et al., 2006), tunable metamaterials (Lee et al., 2012; Rudykh et al., 2014; Wang et al., 2016), to surface engineering (Harrison et al., 2004; Yu et al., 2010; Wang and Xiao, 2017) etc. Motivated with these novel applications, over the last decade, extensive theoretical studies have been performed to explore the underlying mechanism of this phenomenon. The early efforts mainly focus on buckling of a stiff thin film resting on a single-layer, homogenous substrate (Mei et al., 2011; Huang et al., 2005; Jiang et al., 2007; Song et al., 2008; Duan et al., 2008; Dong et al., 2018; Pan et al., 2014; Li et al., 2018; Cheng and Song, 2014). A few works have been carried out for the system of a stiff thin film on a multi-layer compliant substrate, which is frequently observed in practical applications. For instance, the introduction of an additional intermediate thin layer at the interface between the thin film and the substrate can enhance the adhesion of the substrate that is difficult to adhere directly to the stiff thin film (Nolte et al., 2006; Kim et al., 2009). In addition, many living soft tissues (e.g., skins, brain) and chemically or physically treated soft polymers (Befahy et al., 2009) can also be considered as multi-layer, compliant substrates.

For the buckling of a thin film on a multi-layer, inhomogeneous compliant substrate, the stiffness of each layer has significant influence on the buckling configuration of the system. Jia et al. (2012) and Xie et al. (2014) presented analytical studies for a stiff thin film adhered to a bi-layer substrate of infinite thickness and captured several wrinkling modes by modulating the elastic modulus of the intermediate thin layer. Cheng et al. (2014) performed the mechanics analysis for the similar system with the focus on the stretchability of the brittle, thin film. Furthermore, buckling of a stiff thin film on multi-layer (more than three layers) (Lejeune et al., 2016a, 2016b) and elastic graded substrates of infinite thickness (Jia et al., 2014; Chen et al., 2017; Cao et al., 2012) were also analytically investigated. These studies

* Corresponding authors:.
E-mail addresses: chenwq@zju.edu.cn (W. Chen), jzsong@zju.edu.cn (J. Song).
[1] These authors contribute equally to this work.

https://doi.org/10.1016/j.ijsolstr.2019.10.012
0020-7683/

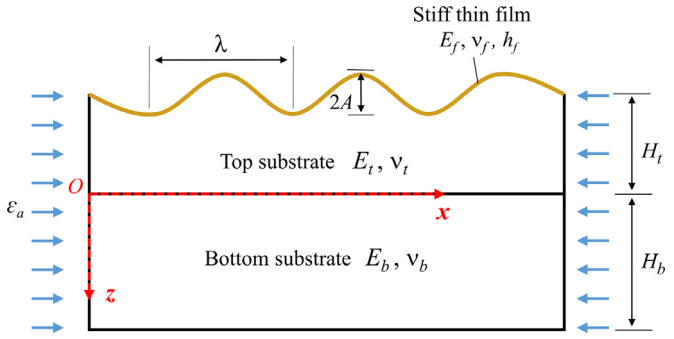

Fig. 1. The schematic diagram of a stiff thin film buckled on a bi-layer compliant substrate of finite thickness.

shed light on surface instabilities of a stiff thin film on an inhomogeneous substrate, however, in their models, a substrate layer of semi-infinite thickness is assumed for simplicity, which is valid in most cases and thus the influence of the finite substrate thickness on the buckling behavior is still unclear.

We aim to study the buckling of a stiff thin film on a bi-layer substrate of finite thickness theoretically, numerically and experimentally. Particularly, the influence of finite thickness of the bi-layer substrate on the buckling behavior is systematically investigated. The paper is outlined as follows. The theoretical model, finite element analysis (FEA), and experiments are described in Section 2, 3 and 4, respectively. Section 5 presents the results and discussion. Section 6 summarizes the main conclusions.

2. Theoretical model of buckling

Fig. 1 shows the schematic diagram of a stiff thin film buckled on a bi-layer compliant substrate of finite thickness under the uniaxial in-plane compression ε_a. The Cartesian coordinate system (O-xz) is established with the origin O located at the interface between the top and bottom substrate layers, the x-axis pointing from left to right and the z-axis pointing from top to bottom. Both the film and substrate are linear elastic materials. The thickness, elastic modulus and Poisson's ratio are denoted by h_f, E_f and ν_f, respectively, for the stiff thin film, H_t, E_t and ν_t for the top substrate, H_b, E_b and ν_b for the bottom substrate. All interfaces are perfectly laminated without any slippage.

2.1. Small-deformation buckling analysis

When the in-plane compression is small, the thin film remains flat. Once the in-plane compression exceeds the critical compression, the thin film buckles with the out-of-plane displacement denoted by the sinusoidal function $w = A\cos(kx)$, where A is the wave amplitude and k is the wavenumber. By following the previous study (Mei et al., 2011), when the in-plane displacement u and deflection w are small, the deformation of the thin film can be modeled by the linear plate equations and the equilibrium condition of the thin film reads as

$$q = \frac{\bar{E}_f h_f^3}{12}\frac{d^4w}{dx^4} - \varepsilon \bar{E}_f h_f \frac{d^2w}{dx^2}, \quad \tau = \bar{E}_f h_f \frac{d^2u}{dx^2}, \tag{1}$$

where $q = q_m\cos(kx)$ and $\tau = \tau_m\sin(kx)$ are the normal and shear stresses at the interface of thin film and bi-layer substrate. ε is the nominal compressive strain in the thin film. Here, the interfacial shear stress between the thin film and bi-layer substrate is taken into account since it plays a significant role when the thickness of the bi-layer substrate is small. The energy method is utilized to establish the theoretical model to obtain the critical buckling wavelength and amplitude. The total energy of the buckled system consists of the bending energy and membrane energy of the thin film, and the elastic energy of the bi-layer substrate. The bending energy U_b and membrane energy U_m of the film per unit length can be derived as (Jiang et al., 2007)

$$U_b = \frac{\bar{E}_f h_f^3}{3}\frac{A^2\pi^4}{\lambda^4}, \quad U_m = \frac{\bar{E}_f h_f}{2}\left(\frac{A^2\pi^2}{\lambda^2} + \varepsilon_a\right)^2, \tag{2}$$

where $\lambda = 2\pi/k$ is the buckling wavelength and $\bar{E}_f = E_f/(1-\nu_f^2)$ is the plane-strain modulus of the stiff thin film. The substrate can be considered as an elastic bi-layer subjected to a prescribed normal and shear stresses at the top surface ($z = -H_t$). The elastic energy of the bi-layer substrate per unit length can be expressed as

$$U_s = \frac{1}{\lambda}\int_0^\lambda \frac{1}{2}\left(\sigma_z^{(t)}w^{(t)}\right)\Big|_{z=-H_t} dx + \frac{1}{\lambda}\int_0^\lambda \frac{1}{2}\left(\tau_{zx}^{(t)}u^{(t)}\right)\Big|_{z=-H_t} dx. \tag{3}$$

Here, $\sigma_z^{(t)}$ and $\tau_{zx}^{(t)}$, $u^{(t)}$ and $w^{(t)}$ are the normal and shear stresses, displacements, respectively, at the top substrate, which will be obtained by solving the plane-strain problem of the elastic bi-layer substrate. The governing equation for each substrate can be written in terms of the Airy stress function F as

$$\nabla^2\nabla^2 F = 0, \tag{4}$$

where $\nabla^2 = \partial^2/\partial x^2 + \partial^2/\partial z^2$ is the two-dimensional Laplacian operator. The Airy stress function F is related to the stresses by

$$\sigma_x = \frac{\partial^2 F}{\partial z^2}, \quad \sigma_z = \frac{\partial^2 F}{\partial x^2}, \quad \tau_{xz} = -\frac{\partial^2 F}{\partial x \partial z}. \tag{5}$$

To exclude both global buckling and rigid-body motions, the boundary conditions for the elastic bi-layer with the bottom fixed can be specified as (Xie et al., 2014)

$$\begin{cases} w^{(t)} = w_m\cos(kx),\ u^{(t)} = u_m\sin(kx) & \text{at } z = 0 \\ \sigma_z^{(t)} = -q_m\cos(kx),\ \tau_{zx}^{(t)} = \tau_m\sin(kx) & \text{at } z = -H_t \end{cases}, \tag{6}$$

and

$$\begin{cases} w^{(b)} = w_m\cos(kx),\ u^{(b)} = u_m\sin(kx) & \text{at } z = 0 \\ w^{(b)} = 0,\ u^{(b)} = 0 & \text{at } z = H_b \end{cases}, \tag{7}$$

with the superscripts (t) and (b) representing the top and bottom substrates, respectively. u_m, w_m, q_m and τ_m are constants, which are to be determined by the interfacial continuity conditions. For the sinusoidal buckling with the out-of-plane displacement $w = A\cos(kx)$, the Airy function takes the form of $F = F_0(z)\cos(kx)$, which can be solved from Eq. (4) as

$$F_0(z) = C_1 e^{kz} + C_2 z e^{kz} + C_3 e^{-kz} + C_4 z e^{-kz}, \tag{8}$$

with C_1, C_2, C_3 and C_4 as coefficients to be determined by boundary conditions.

The substitution of Eq. (8) into Eq. (5) yields the stresses as

$$\sigma_x(x,z) = k\left[(C_1k + 2C_2)e^{kz} + C_2kze^{kz} + (C_3k - 2C_4)e^{-kz} + C_4kze^{-kz}\right]\cos(kx), \tag{9}$$

$$\sigma_z(x,z) = -k^2\left[C_1e^{kz} + C_2ze^{kz} + C_3e^{-kz} + C_4ze^{-kz}\right]\cos(kx), \tag{10}$$

and

$$\tau_{xz}(x,z) = k\left[(C_1k + C_2)e^{kz} + C_2kze^{kz} - (C_3k - C_4)e^{-kz} - C_4kze^{-kz}\right]\sin(kx). \tag{11}$$

According to the linear elastic constitutive model, the displacements can be expressed as $u = U(z)\sin(kx)$ and $w = W(z)\cos(kx)$ with $U(z)$ and $W(z)$ satisfying

$$\frac{E}{(1+\nu)}U(z) = [kC_1 + 2(1-\nu)C_2]e^{kz} + kC_2ze^{kz} + [kC_3 - 2(1-\nu)C_4]e^{-kz} + kC_4ze^{-kz}, \tag{12}$$

and

$$-\frac{E}{(1+\nu)}W(z)=[kC_1+(2\nu-1)C_2]e^{kz}+kC_2ze^{kz}-[kC_3-(2\nu-1)C_4]e^{-kz}-kC_4ze^{-kz}. \quad (13)$$

For the top substrate layer, substituting Eqs. (10)–(13) into the boundary condition in Eq. (6) gives the following linear algebraic equations

$$\begin{bmatrix} k^2e^{-kH_t} & -k^2H_te^{-kH_t} & k^2e^{kH_t} & -k^2H_te^{kH_t} \\ k^2e^{-kH_t} & ke^{-kH_t}(1-kH_t) & -k^2e^{kH_t} & ke^{kH_t}(1+kH_t) \\ k & 2(1-\nu_t) & k & -2(1-\nu_t) \\ -k & 1-2\nu_t & k & 1-2\nu_t \end{bmatrix}\begin{Bmatrix} C_1 \\ C_2 \\ C_3 \\ C_4 \end{Bmatrix} = \begin{Bmatrix} q_m \\ \tau_m \\ \frac{E_t}{1+\nu_t}u_m \\ \frac{E_t}{1+\nu_t}w_m \end{Bmatrix}. \quad (14)$$

The coefficients C_1, C_2, C_3 and C_4 can be obtained in terms of the four unknown constants u_m, w_m, q_m and τ_m by solving Eq. (14). Thus, the normal and shear stresses at the interface of $z=0$, to be used to determine the unknown constants u_m, w_m, q_m and τ_m via the interfacial continuity conditions, can be obtained as

$$\begin{cases} \sigma_z^{(t)}\big|_{z=0} = [k(c_{11}u_m+c_{12}w_m)+c_{13}q_m+c_{14}\tau_m]\cos(kx) \\ \tau_{zx}^{(t)}\big|_{z=0} = [k(c_{21}u_m+c_{22}w_m)+c_{23}q_m+c_{24}\tau_m]\sin(kx) \end{cases}, \quad (15)$$

with $\xi=kH_t$ and

$$\begin{aligned}
c_{11} &= -\frac{(1-2\nu_t)[\cosh(2\xi)-1]+2\xi^2}{(3-4\nu_t)\cosh(2\xi)+2\xi^2+(8\nu_t^2-12\nu_t+5)}\frac{E_t}{1+\nu_t}, \\
c_{12} &= \frac{2(1-\nu_t)[\sinh(2\xi)-2\xi]}{(3-4\nu_t)\cosh(2\xi)+2\xi^2+(8\nu_t^2-12\nu_t+5)}\frac{E_t}{1+\nu_t}, \\
c_{13} &= -\frac{4(1-\nu_t)[\xi\sinh(\xi)+2(1-\nu_t)\cosh(\xi)]}{(3-4\nu_t)\cosh(2\xi)+2\xi^2+(8\nu_t^2-12\nu_t+5)}, \\
c_{14} &= -\frac{4(1-\nu_t)[\xi\cosh(\xi)+(1-2\nu_t)\sinh(\xi)]}{(3-4\nu_t)\cosh(2\xi)+2\xi^2+(8\nu_t^2-12\nu_t+5)} \\
c_{21} &= \frac{2(1-\nu_t)[\sinh(2\xi)+2\xi]}{(3-4\nu_t)\cosh(2\xi)+2\xi^2+(8\nu_t^2-12\nu_t+5)}\frac{E_t}{1+\nu_t}, \\
c_{22} &= c_{11}, \\
c_{23} &= -\frac{4(1-\nu_t)[\xi\cosh(\xi)-(1-2\nu_t)\sinh(\xi)]}{(3-4\nu_t)\cosh(2\xi)+2\xi^2+(8\nu_t^2-12\nu_t+5)}, \\
c_{24} &= -\frac{4(1-\nu_t)[\xi\sinh(\xi)-2(1-\nu_t)\cosh(\xi)]}{(3-4\nu_t)\cosh(2\xi)+2\xi^2+(8\nu_t^2-12\nu_t+5)}.
\end{aligned}$$

The displacements at the top of the substrate ($z=-H_t$), which is useful to calculate the elastic energy of the bi-layer substrate in Eq. (3), can be obtained as

$$u^{(t)}\big|_{z=-H_t}=\left(c_{31}u_m+c_{32}w_m+\frac{1}{k}c_{33}q_m+\frac{1}{k}c_{34}\tau_m\right)\sin(kx), \quad (16)$$

with

$$\begin{aligned}
c_{31} &= -\frac{4(1-\nu_t)[\xi\sinh(\xi)-2(1-\nu_t)\cosh(\xi)]}{(3-4\nu_t)\cosh(2\xi)+2\xi^2+(8\nu_t^2-12\nu_t+5)}, \\
c_{32} &= -\frac{4(1-\nu_t)[\xi\cosh(\xi)+(1-2\nu_t)\sinh(\xi)]}{(3-4\nu_t)\cosh(2\xi)+2\xi^2+(8\nu_t^2-12\nu_t+5)}, \\
c_{33} &= -\frac{(3-10\nu_t+8\nu_t^2)[\cosh(2\xi)-1]-2\xi^2}{(3-4\nu_t)\cosh(2\xi)+2\xi^2+(8\nu_t^2-12\nu_t+5)}\frac{1+\nu_t}{E_t}, \\
c_{34} &= -\frac{2(1-\nu_t)[2\xi+(3-4\nu_t)\sinh(2\xi)]}{(3-4\nu_t)\cosh(2\xi)+2\xi^2+(8\nu_t^2-12\nu_t+5)}\frac{1+\nu_t}{E_t},
\end{aligned}$$

and

$$w^{(t)}\big|_{z=-H_t}=\left(c_{41}u_m+c_{42}w_m+\frac{1}{k}c_{43}q_m+\frac{1}{k}c_{44}\tau_m\right)\cos(kx), \quad (17)$$

with

$$\begin{aligned}
c_{41} &= \frac{4(1-\nu_t)[\xi\cosh(\xi)-(1-2\nu_t)\sinh(\xi)]}{(3-4\nu_t)\cosh(2\xi)+2\xi^2+(8\nu_t^2-12\nu_t+5)}, \\
c_{42} &= \frac{4(1-\nu_t)[\xi\sinh(\xi)+2(1-\nu_t)\cosh(\xi)]}{(3-4\nu_t)\cosh(2\xi)+2\xi^2+(8\nu_t^2-12\nu_t+5)}, \\
c_{43} &= -\frac{2(1-\nu_t)[2\xi-(3-4\nu_t)\sinh(2\xi)]}{(3-4\nu_t)\cosh(2\xi)+2\xi^2+(8\nu_t^2-12\nu_t+5)}\frac{1+\nu_t}{E_t}, \\
c_{44} &= \frac{(3-10\nu_t+8\nu_t^2)[\cosh(2\xi)-1]-2\xi^2}{(3-4\nu_t)\cosh(2\xi)+2\xi^2+(8\nu_t^2-12\nu_t+5)}\frac{1+\nu_t}{E_t}.
\end{aligned}$$

For the bottom substrate layer, we can follow the similar procedure for the top substrate layer to obtain the normal and shear stresses at the interface of $z=0$ as

$$\begin{cases} \sigma_z^{(b)}\big|_{z=0} = (c_{51}u_m+c_{52}w_m)k\cos(kx) \\ \tau_{zx}^{(b)}\big|_{z=0} = (c_{61}u_m+c_{62}w_m)k\sin(kx) \end{cases}, \quad (18)$$

with $\eta=kH_b$ and

$$\begin{aligned}
c_{51} &= -\frac{(8\nu_b^2-10\nu_b+3)\cosh(2\eta)-(2\eta^2+8\nu_b^2-10\nu_b+3)}{(3-4\nu_b)^2\cosh(2\eta)-2\eta^2-(3-4\nu_b)^2}\frac{E_b}{1+\nu_b}, \\
c_{52} &= -\frac{2(1-\nu_b)[(3-4\nu_b)\sinh(2\eta)+2\eta]}{(3-4\nu_b)^2\cosh(2\eta)-2\eta^2-(3-4\nu_b)^2}\frac{E_b}{1+\nu_b}, \\
c_{61} &= -\frac{2(1-\nu_b)[(3-4\nu_b)\sinh(2\eta)-2\eta]}{(3-4\nu_b)^2\cosh(2\eta)-2\eta^2-(3-4\nu_b)^2}\frac{E_b}{1+\nu_b}, \\
c_{62} &= -\frac{(8\nu_b^2-10\nu_b+3)\cosh(2\eta)-(2\eta^2+8\nu_b^2-10\nu_b+3)}{(3-4\nu_b)^2\cosh(2\eta)-2\eta^2-(3-4\nu_b)^2}\frac{E_b}{1+\nu_b}.
\end{aligned}$$

At the interface between the top and bottom substrates, i.e. $z=0$, the continuity conditions require

$$\sigma_z^{(t)}\big|_{z=0}=\sigma_z^{(b)}\big|_{z=0},\quad \tau_{zx}^{(t)}\big|_{z=0}=\tau_{zx}^{(b)}\big|_{z=0}, \quad (19)$$

which yields

$$u_m=\frac{1}{k}(\gamma_{11}q_m+\gamma_{12}\tau_m),\quad w_m=\frac{1}{k}(\gamma_{21}q_m+\gamma_{22}\tau_m), \quad (20)$$

with

$$\begin{aligned}
\gamma_{11} &= \frac{c_{13}(c_{62}-c_{22})-c_{23}(c_{52}-c_{12})}{(c_{51}-c_{11})(c_{62}-c_{22})-(c_{52}-c_{12})(c_{61}-c_{21})}, \\
\gamma_{12} &= \frac{c_{14}(c_{62}-c_{22})-c_{24}(c_{52}-c_{12})}{(c_{51}-c_{11})(c_{62}-c_{22})-(c_{52}-c_{12})(c_{61}-c_{21})}, \\
\gamma_{21} &= \frac{c_{23}(c_{51}-c_{11})-c_{13}(c_{61}-c_{21})}{(c_{51}-c_{11})(c_{62}-c_{22})-(c_{52}-c_{12})(c_{61}-c_{21})}, \\
\gamma_{22} &= \frac{c_{24}(c_{51}-c_{11})-c_{14}(c_{61}-c_{21})}{(c_{51}-c_{11})(c_{62}-c_{22})-(c_{52}-c_{12})(c_{61}-c_{21})}.
\end{aligned}$$

Inserting Eqs. (16) and (17) into Eq. (1) yields the relation between q_m and τ_m, namely

$$(c_{31}\gamma_{11}+c_{32}\gamma_{21}+c_{33})q_m+\left(\frac{1}{\bar{E}_f k h_f}+c_{31}\gamma_{12}+c_{32}\gamma_{22}+c_{34}\right)\tau_m=0. \quad (21)$$

At the interface between the thin film and bi-layer substrate, i.e. $z=-H_t$, the continuity of deflection gives

$$c_{41}u_m+c_{42}w_m+\frac{1}{k}c_{43}q_m+\frac{1}{k}c_{44}\tau_m=A. \quad (22)$$

By combining Eqs. (20)–(22), we can obtain the normal and shear stresses, displacement at the top of the bi-layer substrate in terms of the buckling amplitude A as,

$$\sigma_z^{(t)}\big|_{z=-H_t} = \chi A k \cos(kx), \quad \tau_{zx}^{(t)}\big|_{z=-H_t} = \chi\zeta A k \sin(kx),$$
$$u^{(t)}\big|_{z=-H_t} = \chi(\gamma_{11}+\zeta\gamma_{12})A\sin(kx). \tag{23}$$

with

$$\chi = [c_{41}\gamma_{11}+c_{42}\gamma_{21}+c_{43}+\zeta(c_{41}\gamma_{12}+c_{42}\gamma_{22}+c_{44})]^{-1},$$
$$\zeta = -(c_{31}\gamma_{11}+c_{32}\gamma_{21}+c_{33})\left(\frac{1}{\bar{E}_f k h_f}+c_{31}\gamma_{12}+c_{32}\gamma_{22}+c_{34}\right)^{-1}.$$

Inserting Eq. (23) into Eq. (3) yields the strain energy per unit length in the substrate as

$$U_s = \bar{E}_t g_c \frac{\pi A^2}{2\lambda}, \tag{24}$$

with $g_c = \frac{\chi}{\bar{E}_t}[1+\chi\zeta(\gamma_{11}+\zeta\gamma_{12})]$.

The minimization of the total energy $U_{\text{total}} = U_b + U_m + U_s$ with respect to the buckling wavelength λ and amplitude A gives

$$\lambda_c = 2\pi h_f\left[\frac{\bar{E}_f}{6(\alpha+1)g_c\bar{E}_t}\right]^{\frac{1}{3}}, \quad A = h_f\sqrt{\frac{1}{3}\frac{\alpha+3}{\alpha+1}\left(\frac{\varepsilon_a}{\varepsilon_c}-1\right)}, \tag{25}$$

where ε_c is the critical buckling strain given by

$$\varepsilon_c = \frac{1}{12}\frac{\alpha+3}{\alpha+1}\left[\frac{6(1+\alpha)g_c\bar{E}_t}{\bar{E}_f}\right]^{\frac{2}{3}}, \tag{26}$$

and $\alpha = \lambda\frac{1}{g_c}\frac{dg_c}{d\lambda}$ is a non-dimensional factor. It is observed that the buckling wavelength is independent of the in-plane compression, which is consistent for the buckling analysis of a stiff thin film on a homogeneous compliant substrate (Huang et al., 2005; Jiang et al., 2007; Song et al., 2008). This compression-independent buckling wavelength is also called the critical buckling wavelength and is written as λ_c. It should be also noted that the above analytical expressions can degenerate to previous solutions for a stiff thin film buckled on a semi-infinite single-layer (Huang et al., 2005) or bi-layer substrate of infinite thickness (Jia et al., 2012), which will be further discussed in the section of results and discussion.

2.2. Finite-deformation buckling analysis

The results in Section 2.1 are only good for a relatively small in-plane compression ε_a since they are obtained under the assumption of small deformation. The predicted compression-independent wavelength in Eq. (25) is not valid anymore for a relatively large in-plane compression ε_a. To obtain the buckled configuration under a relatively large compression, a finite-deformation theory is critically needed. Cheng and Song (2014) showed that finite geometry change dominates in the finite-deformation theory for buckling of a stiff thin film on a compliant substrate while the influences of finite strain and nonlinear constitutive relationship of the substrate are negligible. It is reasonable to adopt the above conclusion for the buckling analysis of a stiff thin film on a bi-layer compliant substrate considering the similarity between the two systems. In this section, a simple theoretical model is established to predict the buckling configuration of the stiff thin film on a bi-layer compliant substrate at various applied in-plane compression ε_a by accounting for finite geometry change via the energy method.

The bending energy U_b and membrane energy U_m of the film per unit length become (Cheng and Song, 2014)

$$U_b = \frac{\bar{E}_f h_f^3}{3(1+\varepsilon_a)^4}\frac{A^2\pi^4}{\lambda^4},$$

$$U_m = \frac{\bar{E}_f h_f}{2}\left(\frac{A^2\pi^2}{\lambda^2(1+\varepsilon_a)^2}-\frac{\varepsilon_a}{1+\varepsilon_a}\right)^2. \tag{27}$$

The elastic energy of the bi-layer substrate becomes

$$U_s = \frac{\bar{E}_t g_c}{1+\varepsilon_a}\frac{\pi A^2}{2\lambda}. \tag{28}$$

Thus, the buckled configuration can be determined by minimizing the total energy with respect to the wavelength and amplitude as

$$\lambda_c = \frac{2\pi h_f}{1+\varepsilon_a}\left(\frac{\bar{E}_f}{6(\alpha+1)g_c\bar{E}_t}\right)^{\frac{1}{3}}, \quad A = h_f\sqrt{\frac{1}{3}\frac{\alpha+3}{\alpha+1}\left(\frac{\varepsilon_a}{(1+\varepsilon_a)\varepsilon_c}-1\right)}, \tag{29}$$

which indicates that the buckling wavelength decreases with the increase of the applied compression.

3. Finite element analysis

A plane-strain finite element model is established to study the nonlinear buckling behavior of a stiff thin film on a bi-layer compliant substrate in ABAQUS and to validate the theoretical model. The plane-strain element (CPE4) and beam element (B21) are selected to discretize the substrate and film, respectively and the linear elastic constitutive relation is used to model both the stiff thin film and the bi-layer substrate. The length of the model is large enough (more than 20 times the buckling wavelength) to eliminate the influences of the left and right end boundaries. The in-plane compression is directly applied to the system through the displacements on the left and right ends, which is the same as the analytical modeling. The large differences in elastic modulus and thickness of the film and substrate require a fine mesh near the film/substrate interface to ensure the convergence of finite element analysis. The element size near the film/substrate interface is set as about 1/5 film thickness and it increases as the distance to the interface increases.

The Buckling function in ABAQUS is used to obtain the critical buckling wavelength and strain (i.e., the first eigenmode and its associated eigenvalue) for the stiff thin film on a bi-layer compliant substrate. To trigger the buckling of the film/substrate system, the first eigenmode is selected as the tiny geometric imperfection (smaller than 0.1% of film thickness) in the postbuckling analysis. The dependence of buckling configuration on the in-plane compression is then obtained by the Static function in ABAQUS.

4. Experiments

To validate the theoretical model for buckling of a stiff thin film on a bi-layer compliant substrate, we also carried out experiments by selecting silicon nanoribbon as the film and polydimethylsiloxane (PDMS) as the substrate to fabricate the film/substrate system. The fabrication of the bottom (or top) PDMS substrate begins with the mixing of pre-polymer and cross-linker at the weight ratio of 10:1 (or 20:1) followed by the spin-coating on a glass slide and the curing at the temperature of 100 °C for one hour. The resulting bottom and top PDMS substrates have the elastic moduli of 1.54 MPa and 0.42 MPa measured by the Dynamic Mechanical Analyzer (TA Instruments, DMA Q800), respectively, at a 2% strain per minute. The PDMS thickness is determined by the spin-coating speed. For the top PDMS substrate, the spinning speeds of 1500 rpm and 4000 rpm yield the thicknesses of 30 μm and 14 μm, respectively. For the bottom PDMS substrate, mold casting method is used to give a thickness of 2000 μm. The top and bottom PDMS substrates experience an oxygen plasma surface treatment before they are chemically bonded. After the bi-layer PDMS substrate is

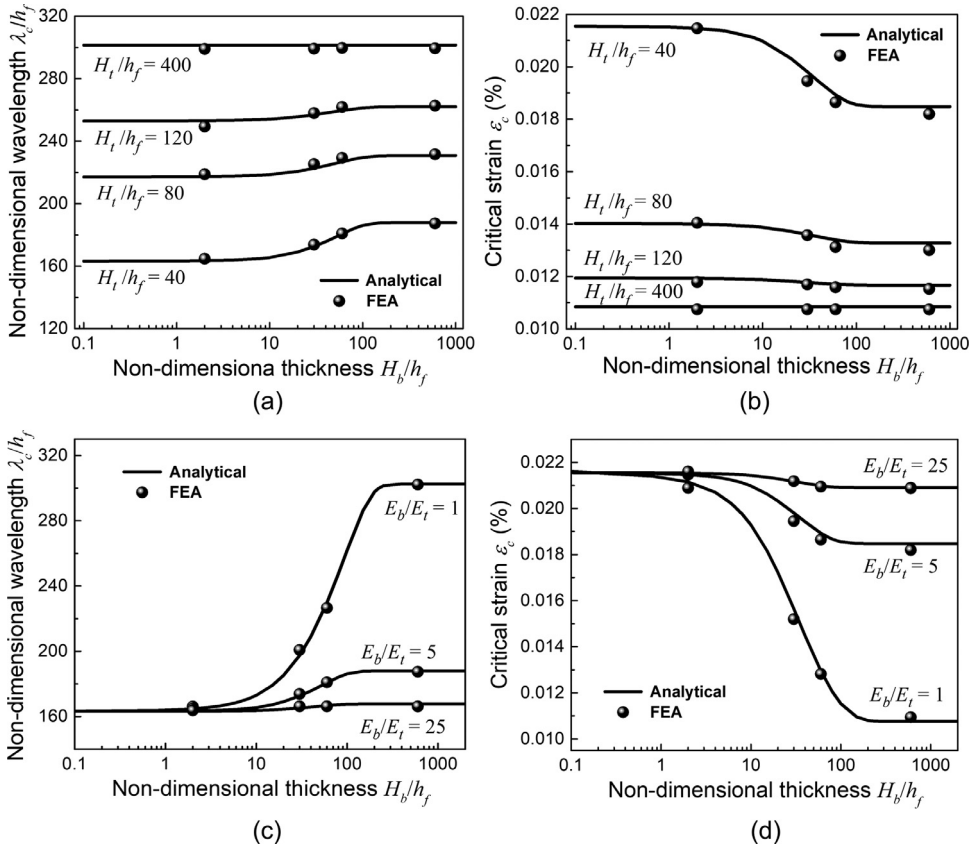

Fig. 2. The non-dimensional buckling wavelength (a) and critical strain (b) as functions of the non-dimensional thickness of the bottom substrate under various thicknesses of the top substrate for E_b/E_t=5. The non-dimensional buckling wavelength (c) and critical strain (d) as functions of the non-dimensional thickness of the bottom substrate under various substrate modulus ratios for H_t/h_f=40. Here ν_f=0.27, ν_t=ν_b=0.48 and E_f/E_t=400000.

fabricated, the silicon nanoribbon of 180 nm thickness harvested from a SOI wafer is transfer printed onto the pre-stretched bi-layer PDMS substrate slabs with the in-plane size of 20 mm × 10 mm. Upon releasing the pre-strain of the bi-layer substrate at a 5% strain per minute, the silicon nanoribbon buckles to form the sinusoidal wave with the wavelength and amplitude measured by a step profilometer (Bruker DektakXT, GER). Although the experimental setting is different from the modeling, where the pre-strain of the substrate is applied and released in experiments while the direct compression to the whole system is applied in modeling, it is reasonable since the difference is negligible under either applying the pre-strain of the substrate or the direct compression of the system for the large stiffness ratio of the stiff thin film and the soft substrate larger than 100 (Holland et al., 2017).

5. Results and discussion

By a dimensional consideration, the critical buckling strain ε_c in Eq. (26) can be written as

$$\varepsilon_c=\varepsilon_c\left(\frac{E_f}{E_t}, \frac{E_b}{E_t}, \frac{H_t}{h_f}, \frac{H_b}{h_f}, \nu_f, \nu_t, \nu_b\right), \tag{30}$$

which clearly indicates that the critical buckling strain depends on seven non-dimensional parameters, i.e., the ratio of the elastic modulus (E_f/E_t and E_b/E_t), the ratio of the thickness (H_t/h_f and H_b/h_f), and the Poisson's ratio (ν_f, ν_t and ν_b). Similarly, the normalized critical buckling wavelength $\bar{\lambda}_c=\lambda_c/h_f$ also depends on seven non-dimensional parameters, i.e.,

$$\bar{\lambda}_c=2\pi\left(\frac{\bar{E}_f}{6(\alpha+1)g_c\bar{E}_t}\right)^{\frac{1}{3}}=\bar{\lambda}_c\left(\frac{E_f}{E_t}, \frac{E_b}{E_t}, \frac{H_t}{h_f}, \frac{H_b}{h_f}, \nu_f, \nu_t, \nu_b\right). \tag{31}$$

To clearly show the influence of finite thickness of bi-layer substrate on the buckling behavior of the stiff thin film on the bi-layer compliant substrate, the Poisson's ratios are set as ν_f=0.27 for the silicon film and ν_t=ν_b=0.48 for the PDMS substrate. Fig. 2a and 2b show the non-dimensional buckling wavelength and critical buckling strain as functions of the non-dimensional thickness of the bottom substrate under various non-dimensional thicknesses of the top substrate. The modulus ratios are set as E_f/E_t=400000 and E_b/E_t=5. It's observed that the non-dimensional thicknesses of H_t/h_f and H_b/h_f have significant influences on both the buckling wavelength and critical strain. For H_t/h_f within the range from 40 to 400, a thicker top substrate leads to a larger buckling wavelength but a smaller critical strain. When the top substrate is thick (over a few hundred times the film thickness), both the buckling wavelength and the critical buckling strain are independent of the thickness of the bottom substrate. This is because the bi-layer substrate will degenerate to a single-layer substrate and the critical buckling condition is completely determined by the elastic properties of the film and top substrate. When the top substrate is thin, the buckling wavelength remains unchanged with the increase of the bottom substrate thickness for a thin (about the film thickness) bottom substrate, then experiences a slight increase (~ 10%) for an intermediate thick bottom substrate, and finally reaches a steady value for a thick (over one hundred times the film thickness) bottom substrate. The critical buckling strain has a similar

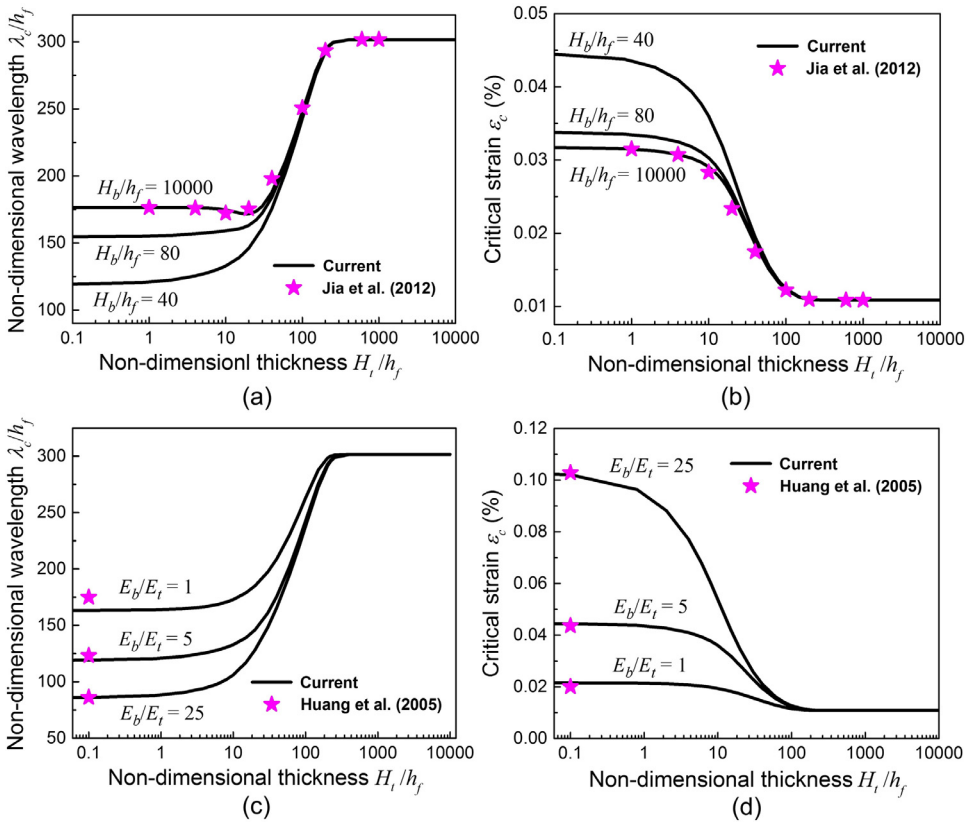

Fig. 3. The non-dimensional buckling wavelength (a) and critical strain (b) as functions of the non-dimensional thickness of the top substrate, under various thicknesses of the bottom substrate for E_b/E_t=5. The non-dimensional buckling wavelength (c) and critical strain (d) as functions of the non-dimensional thickness of the top substrate under various substrate modulus ratios for H_b/h_f=40. Here ν_f=0.27, ν_t=ν_b=0.48 and E_f/E_t=400000.

trend except a slight decrease for an intermediate thick bottom substrate. In order to validate the theoretical predictions, the results denoted by the solid dot from finite element analysis are also shown in Fig. 2a and Fig. 2b. The good agreement between finite element analysis and theoretical predictions (even for the extremely thin bi-layer substrate) validates the theoretical model (small-deformation).

The influences of substrate modulus ratio E_b/E_t on the buckling wavelength and the critical strain are studied under E_f/E_t=400000 and $H_t/h_f = 40$ as shown in Fig. 2c and 2d. As we can see, the elastic modulus ratio E_b/E_t has a significant effect on the buckling behavior of the system. The increase of E_b/E_t can rapidly decrease the buckling wavelength or increase the critical buckling strain. As expected, the effect of E_b/E_t will vanish when the bottom substrate thickness is very thin. As the bottom substrate thickness increases, the buckling wavelength firstly increases while the critical buckling strain firstly decreases and then both reach steady values once the bottom substrate thickness is over one hundred times the film thickness. This can be easily understood since the influence of the bottom substrate thickness vanishes for a thick bottom substrate.

To investigate the effect of finite thickness of the top substrate, we plot the non-dimensional buckling wavelength and the critical buckling strain as functions of the non-dimensional thickness of the top substrate under various non-dimensional thicknesses of the bottom substrate in Fig. 3a and 3b. The modulus ratios are set as E_f/E_t=400000 and E_b/E_t=5. It is shown again that both the buckling wavelength and critical buckling strain are independent of the bottom substrate thickness when the top substrate thickness is over a few hundred times the film thickness. The effects of the top substrate thickness are negligible for either very thin (∼ one time the film thickness) or very thick (a few hundred times the film thickness) top substrate. While for an intermediate thick top substrate, the increase of the top substrate thickness increases the buckling wavelength and decreases the critical buckling strain significantly. Particularly, when the bottom substrate is very thick ($H_b/h_f = 10000$), the present solution can degenerate to the model developed by Jia et al. (2012), for a stiff thin film buckled on a bi-layer substrate of infinite thickness.

The effects of substrate modulus ratio E_b/E_t on the buckling wavelength and the critical strain under E_f/E_t=400000 and H_b/h_f=40 are shown in Fig. 3c and 3d. The increase of E_b/E_t decreases the buckling wavelength and increases the critical buckling strain. This effect vanishes when the top substrate thickness is very large (over one hundred times film thickness) due to the complete separation of the film buckling from the bottom substrate. When the top substrate is very thin (about one time film thickness), the effect of the top substrate is negligible and the results degenerate to the model of a stiff thin film on a single-layer compliant substrate of finite thickness (Huang et al., 2005). The slight difference between the two analytical results lies in the assumption in the theoretical model developed by Huang et al. (2005), e.g., no shear at the film/substrate interface.

Fig. 4 shows the buckling configuration of the silicon nanoribbon on the bi-layer compliant PDMS substrate at various applied strains. The bottom PDMS substrate is 2000 μm. Two thicknesses of the top PDMS substrate including 14 μm and 30 μm are considered. The optical and SEM images in Fig. 4a and the measured surface profile in Fig. 4b of the buckled silicon nanoribbon show a well-defined, periodic buckling pattern with the out-of-plane displacement in a form of sinusoidal function, which validates

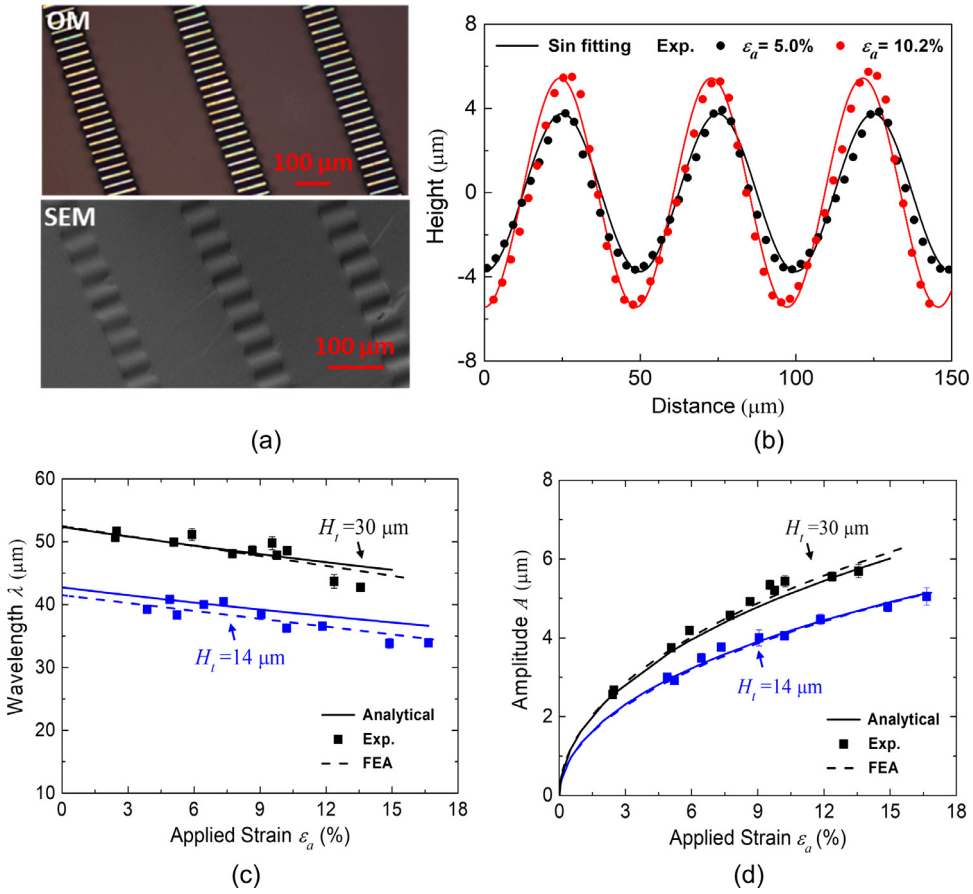

Fig. 4. The buckling configuration of the silicon nanoribbon on the bi-layer compliant PDMS substrate under various applied strains. (a) Optical microscope image (OM) and scanning electron microscope image (SEM), and (b) the measured and fitted sinusoidal profile of the buckled silicon nanoribbons on the bi-layer compliant PDMS substrate for the thickness of the top substrate of 30 μm. (c) The buckling wavelength and (d) amplitude as functions of the applied strain under various top substrate thicknesses of 14 μm and 30 μm with the material and geometry parameters E_f=130 GPa, ν_f=0.27, h_f=180 nm, E_t = 0.4237 MPa,ν_f=0.48, E_b = 1.5247 MPa, ν_b=0.48, H_b=2000 μm.

the theoretical assumption in Section 2. The comparison of the wavelength and amplitude from the theoretical prediction (finite-deformation), finite element analysis and experimental measurement shows a good agreement among each other as shown in Fig. 4c and 4d, which indicates the developed finite-deformation theory works well to predict the morphology evolution of a stiff thin film on a bi-layer substrate of finite thickness.

6. Conclusions

A theoretical model, validated by finite element analysis and experiment, is established for the buckling of a stiff thin film on a bi-layer compliant substrate of finite thickness. Both small-deformation buckling analysis and finite-deformation buckling analysis accounting for finite geometry change are performed. The influences of finite thickness of the bi-layer substrate and the substrate modulus ratio on the buckling wavelength and critical buckling strain are systematically investigated. It is shown that the bi-layer substrate can degenerate to a single layer substrate for very thin or very thick top substrate. The quantitative agreement of buckling behavior among the theoretical prediction, finite element analysis and experimental measurement validates the theoretical model. These results are helpful to understand surface buckling of the stiff thin film on the bilayer substrate and are of importance to provide design guidelines for stretchable electronics, micro- and nano-metrology, and surface engineering involving the bi-layer substrate-supported thin film buckling.

Acknowledgements

The authors acknowledge the supports from the National Basic Research Program (Grant No. 2015CB351901), the National Natural Science Foundation of China (Grant Nos. 11622221, 11872331, and 11621062), the Shenzhen Science and Technology Program (Grant No. JCY20170816172454095), and the Fundamental Research Funds for the Central Universities.

Supplementary materials

Supplementary material associated with this article can be found, in the online version, at doi:10.1016/j.ijsolstr.2019.10.012.

References

Befahy, S., Lipnik, P., Pardoen, T., Nascimento, C., Patris, B., Bertrand, P., Yunus, S., 2009. Thickness and elastic modulus of plasma treated PDMS silica-like surface layer. Langmuir 26, 3372–3375.
Bowden, N., Brittain, S., Evans, A.G., Hutchinson, J.W., Whitesides, G.M., 1998. Spontaneous formation of ordered structures in thin films of metals supported on an elastomeric polymer. Nature 393, 146–149.
Cao, Y., Jia, F., Zhao, Y., Feng, X., Yu, S., 2012. Buckling and post-buckling of a stiff film resting on an elastic graded substrate. Int. J. Solids Struct. 49, 1656–1664.
Chen, Z., Chen, W., Song, J., 2017. Buckling of a stiff thin film on an elastic graded compliant substrate. Proc. Roy. Soc. A: Math. Phys. Eng. Sci. 473, 20170410.
Cheng, H., Song, J., 2014. A simply analytic study of buckled thin films on compliant substrates. J. App. Mech. 81, 024501.
Cheng, H., Zhang, Y., Hwang, K.C., Rogers, J.A., Huang, Y., 2014. Buckling of a stiff thin film on a pre-strained bi-layer substrate. Int. J. Solids Struct. 51, 3113–3118.

Dong, J., Ma, X., Zhuge, Y., Mills, J.E., 2018. Local buckling of thin plate on tensionless elastic foundations under interactive uniaxial compression and shear. Theor. App. Mech. Lett. 8, 75–82.
Duan, Y., Huang, Y., Yin, Z., 2008. Competing buckling of micro/nanowires on compliant substrates. J. Phys. D: App. Phys. 48, 045302.
Harrison, C., Stafford, C.M., Zhang, W., Karim, A., 2004. Sinusoidal phase grating created by a tunably buckled surface. App. Phys. Lett. 85, 4016–4018.
Holland, M.A., Li, B., Feng, X.Q., Kuhl, E., 2017. Instabilities of soft films on compliant substrates. J. Mech. Phys. Solids 98, 350–365.
Huang, Z.Y., Hong, W., Suo., Z., 2005. Nonlinear analyses of wrinkles in a film bonded to a compliant substrate. J. Mech. Phys. Solids 53, 2101–2118.
Jia, F., Cao, Y.P., Liu, T.S., Jiang, Y., Feng, X.Q., Yu, S.W., 2012. Wrinkling of a bilayer resting on a soft substrate under in-plane compression. Philos. Mag. 92, 1554–1568.
Jia, F., Cao, Y., Zhao, Y., Feng, X., 2014. Buckling and surface wrinkling of an elastic graded cylinder with elastic modulus arbitrarily varying along radial direction. Int. J. App. Mech. 6, 1450003.
Jiang, H., Khang, D.Y., Song, J., Sun, Y., Huang, Y., Rogers, J.A., 2007. Finite deformation mechanics in buckled thin films on compliant supports. Proc. Nat. Acad. Sci. 104, 15607–15612.
Khang, D.Y., Jiang, H., Huang, Y., Rogers, J.A., 2006. A stretchable form of single-crystal silicon for high-performance electronics on rubber substrates. Science 311, 208–212.
Kim, D.H., Ahn, J.H., Choi, W.M., Kim, H.S., Kim, T.H., Song, J., Huang, Y., Liu, Z., Lu, C., Rogers, J.A., 2008. Stretchable and foldable silicon integrated circuits. Science 320, 507–511.
Kim, D.H., Kim, Y.S., Wu, J., Liu, Z., Song, J., Kim, H.S., Huang, Y., Hwang, K.C., Rogers, J.A., 2009. Ultrathin silicon circuits with strain-isolation layers and mesh layouts for high-performance electronics on fabric, vinyl, leather, and paper. Adv. Mat. 21, 3703–3707.
Lee, S., Kim, S., Kim, T.T., Kim, Y., Choi, M., Lee, S.H., Kim, J.Y., Min, B., 2012. Reversibly stretchable and tunable terahertz metamaterials with wrinkled layouts. Adv. Mater. 24, 3491–3497.
Lejeune, E., Javili, A., Linder, C., 2016a. Understanding geometric instabilities in thin films via a multi-layer model. Soft Matter 12, 806–816.
Lejeune, E., Javili, A., Linder, C., 2016b. An algorithmic approach to multi-layer wrinkling. Extreme Mech. Lett. 7, 10–17.
Li, M., Qin, H., Liu, J., Liu, Y., 2018. Mechanism of three-dimensional surface wrinkle manipulation on a compliant substrate. J. App. Mech. 85, 071004.
Mei, H., Landis, C.M., Huang, R., 2011. Concomitant wrinkling and buckle-delamination of elastic thin films on compliant substrates. Mech. Mater. 43, 627–642.
Nolte, A.J., Cohen, R.E., Rubner, M.F., 2006. Effect of relative humidity on the young's modulus of polyelectrolyte multilayer films and related nonionic polymers. Macromolecules 38, 5367–5370.
Pan, K., Ni, Y., He, L., Huang, R., 2014. Nonlinear analysis of compressed elastic thin films on elastic substrates: From wrinkling to buckle-delamination. Int. J. Solids Struct. 51, 21–22.
Rudykh, S., Boyce, M.C., 2014. Transforming wave propagation in layered media via instability-induced interfacial wrinkling. Phys. Rev. lett. 112, 034301.
Song, J., 2015. Mechanics of stretchable electronics. Curr. Opin. Solid State Mater. Sci. 19, 160–170.
Song, J., Feng, X., Huang, Y., 2015. Mechanics and thermal management of stretchable inorganic electronics. Nat. Sci. Rev. 3, 128–143.
Song, J., Jiang, H., Liu, Z., Khang, D.Y., Huang, Y., Rogers, J.A., Lu, C., Koh, C.G., 2008. Buckling of a stiff thin film on a compliant substrate in large deformation. Int. J. Solids Struct. 45, 3107–3121.
Stafford, C.M., Harrison, C., Beers, K.L., Karim, A., Amis, E.J., VanLandingham, M.R., Kim, H.C., Volksen, W., Miller, R.D., Simonyi, E.E., 2004. A buckling-based metrology for measuring the elastic moduli of polymeric thin films. Nat. Mat. 3, 545–550.
Wang, Y., Chen, Y., Li, H., Li, X., Chen, H., Su, H., Lin, Y., Xu, Y., Song, G., Feng, X., 2016. Buckling-based method for measuring the strain–photonic coupling effect of GaAs nanoribbons. ACS Nano 10, 8199–8206.
Wang, Y., Xiao, J., 2017. Programmable, reversible and repeatable wrinkling of shape memory polymer thin films on elastomeric substrates for smart adhesion. Soft Matter 13, 5317–5323.
Wilder, E.A., Guo, S., Lin-Gibson, S., Fasolka, M.J., Stafford, C.M., 2006. N-Aryl acylureas as intermediates in sequential self-repetitive reactions to form poly(amide−imide)s. Macromolecules 39, 12–14.
Xie, W.H., Huang, X., Cao, Y.P., Li, B., Feng, X.Q., 2014. Buckling and postbuckling of stiff lamellae in a compliant matrix. Compos. Sci. Technol. 99, 89–95.
Yu, C., O'Brien, K., Zhang, Y.H., Yu, H., Jiang, H., 2010. Tunable optical gratings based on buckled nanoscale thin films on transparent elastomeric substrates. App. Phys. Lett. 96, 041111.
Zhang, Y.H., Huang, Y.G., Rogers, J.A., 2015. Mechanics of stretchable batteries and supercapacitors. Curr. Opin. Solid State Mat. Sci. 19, 190–199.